Measurements and Analysis of Large-Scale Fading Characteristics in Curved Subway Tunnels at 920 MHz, 2400 MHz, and 5705 MHz

Ke Guan, Bo Ai, Zhangdui Zhong, Carlos F. López, Lei Zhang, Cesar Briso-Rodríguez, Andrej Hrovat, Bei Zhang, Ruisi He, and Tao Tang,

***Abstract*—Wave propagation characteristics in curved tunnels are of importance for designing reliable communications in subway systems. This paper presents the extensive propagation measurements conducted in two typical types of subway tunnels—traditional arched "Type I" tunnel and modern arched "Type II" tunnel—with 300- and 500-m radii of curvature with different configurations—horizontal and vertical polarizations at 920, 2400, and 5705 MHz, respectively. Based on the measurements, statistical metrics of propagation loss and shadow fading (path-loss exponent, shadow fading distribution, autocorrelation, and cross-correlation) in all the measurement cases are extracted. Then, the large-scale fading characteristics in the curved subway tunnels are compared with the cases of road and railway tunnels, the other main rail traffic scenarios, and some "typical" scenarios to give a comprehensive insight into the propagation in various scenarios where the intelligent transportation systems are deployed. Moreover, for each of the large-scale fading parameters, extensive analysis and discussions are made to reflect the physical laws behind the observations. The quantitative results and findings are useful to realize intelligent transportation systems in the subway system.**

***Index Terms*—Propagation loss, propagation measurement, shadow fading, subway tunnel.**

This work was supported in part by the National Natural Science Foundation of China under Grant U1334202 and Grant 61222105, by the 863 Program under Grant 2014AA01A706, by the Fundamental Research Funds for the Central Universities under Grant 2014RC018 and Grant 2014JBZ021, by the State Key Laboratory of Rail Traffic Control and Safety Project under Grant RCS2014ZT32, and by the Spanish Ministry of Economy and Competitiveness through the INNPACTO TECRAIL research Project under Grant IPT-2011-1034-37000.

I. Introduction

As the world acknowledged low-energy consuming "green transportation," rail traffic is widely treated as the fundamental solution for the improvement of the public transportation situations of countries and cities all over the world. Due to a great deal of urban traffic pressure, improving the efficiency and capacity of subway system is an increasing demand. In order to ensure safe operation of the subway, a large number of studies on intelligent transportation system (ITS) applications have been conducted [2]–[5]. Various kinds of wireless communication technologies employed for metropolitan subway system play a significant role to ensure personnel safety, enhance operational efficiency, and process optimization. No matter for public wireless communication systems or signaling and train control communication systems deployed in tunnels, 900 MHz, 2.4 GHz, and 5.8 GHz are three "hot" frequency bands. Hence, the information on propagation characteristics at these three frequency bands is with high interest for both industry and academia of ITS. At 900 MHz frequency band, there are GSM (Global System for Mobile Communications), GSM-R (Global System for Mobile Communications for Railway) [6], LTE (Long Term Evolution), TETRA (Terrestrial Trunked Radio) [7], [8], and LTE-R (Long Term Evolution for Railway) [9]. At 2.4 GHz frequency band, there are Wi-Fi (Wireless Fidelity), UMTS (Universal Mobile Telecommunications System), LTE, CBTC (Communication Based Train Control System) [10], and LTE-R (pending). At 5.8 GHz, there are many wireless radio system deployments based on WLAN (wireless local area network) to realize driverless underground systems, such as in New-York, line 1 in Paris, Malaga, Marmaray, Singapore, etc. [11]. All these communication systems are essentially a key factor for the new generations of ITS [12]–[15].

In order to calculate the number and position of base stations (access points) and predict the radio coverage of these wireless communication systems in subway tunnels, there have been several studies analyzing propagation of UHF (ultra-high frequency: 300 MHz–3 GHz) and SHF (super high frequency: 3 GHz–30 GHz) radio signals in tunnels in the last decades. For the measurements, authors of [16]–[19] presented the measurement results of propagation characteristics in circular tunnels at 450 MHz and 900 MHz, arched railway and road tunnels at 400 MHz, arched railway tunnels at 900 MHz, subway

tunnels at 2.4 GHz, respectively. For the modeling approaches, many researchers proposed modal analysis based on waveguide theory [20], models based on geometrical optics (GO) approach [21], [22] , numerical models based on vector parabolic equation (VPE) techniques [23], and empirical and stochastic models [24] based on measurements (two-slope models [25], [26], three-slope model [27], four-slope model [17], [28], five-zone models [29]–[31], etc.). Both these experimental and theoretical studies systemically form the understanding of wave propagation in tunnels. However, most of these results focus on the straight tunnels. Comparatively speaking, the research on the propagation in curved tunnels are still limited. Authors of [11], [32]–[38] developed simulators based on ray launching or ray tracing approaches for the radio wave propagation in curved tunnels with some specific cross sections, respectively. Authors of [39] simulated the propagation loss in curved tunnels by the theoretical deduction of modal analysis. Authors of [40], [41] predicted the loss for curved tunnels by using the parabolic equation (PE) along with the alternate direction implicit (ADI) method. Author of [42], [43] simulated the attenuation in curved tunnels by employing hybrid modeling approaches.

In summary, most of the existing research on the tunnel curve make the contributions on modeling methods and simulator development, the measurement results concentrate in road, mine, and railway tunnels with specific cross sections at specific frequencies [44], [45]. The measurement results in curved subway tunnels (which are with different cross section sizes and dimensions, wall roughness and materials, and floor structure from road, railway, and mine tunnels) are still rarely presented. This limits the validation of the corresponding simulators and the deployment of wireless communication systems in subway tunnels.

This paper presents a series of comprehensive propagation measurements in various subway tunnels with different configurations. The large-scale fading characterization supplies the first-hand information, and can be used for network planning, channel modeling, key techniques (such as soft handover, macro-diversity, link adaptation, etc.) evaluation, and validation for simulators of different wireless communication systems deployed in tunnel environment at various frequencies.

The rest of this study is organized as follows. The measurement campaign is introduced in Section II. The measurements are made in two typical traditional curved arched "Type I" and modern curved arched "Type II" tunnels. The radii of curvature are 300 m and 500 m, which are typical values of subway tunnels. Corresponding to the three hot frequency bands, frequencies at 920 MHz, 2400 MHz, and 5705 MHz with horizontal and vertical polarizations are used in the measurements. In Section III, the measurement results and large-scale fading parameters (path loss exponent, shadow fading distribution, autocorrelation, and cross-correlation) extraction are presented. Then, in Section IV, based on the parameter extraction from the measurement results, the large-scale fading characteristics of wave propagation in curved arched tunnels are quantitatively analyzed, and finally summarized in a series of tables. Afterwards, corresponding discussions are made in Section V. Section VI draws conclusions.

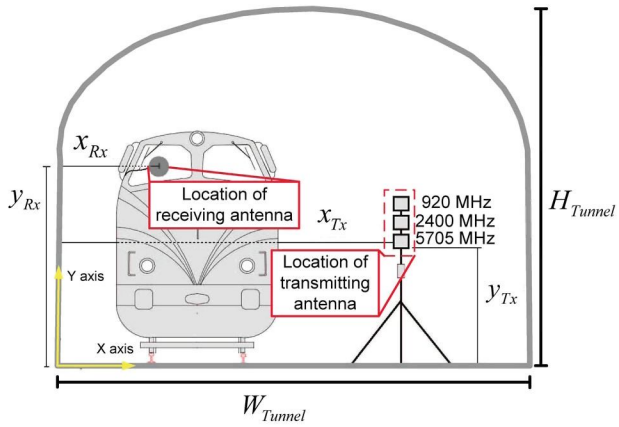

Fig. 1. Front view of the measurement setup in the arched "Type I" tunnel.

II. Measurement Campaign

A. Test System

The test system is composed of the transmitting part and the receiving part as follows:

1) Transmitting system: The transmitting system is comprised of a continuous wave (CW) transmitter (Tx) and a panel antenna. Since three distinguished interesting frequencies are measured, three transmitters and corresponding antennas are utilized. For the measurements at 920 MHz, a Tx with 500 mW (27 dBm) power output, and a L-COM HG908 panel antenna working at the frequency band 902–928 MHz, with 8 dBi gain, 75° horizontal and 65° vertical beam widths are used. In the measurements at 2400 MHz, a Tx with 250 mW (24 dBm) power output is employed to be the Tx; a L-COM HG2414P panel antenna working at the frequency band 2400–2500 MHz, with 14 dBi gain, 30° horizontal and 30° vertical beam widths is utilized. In the cases of 5705 MHz, the Tx is a transmitter with 160 mW (22 dBm) power output; the antenna is a L-COM HG5419P panel antenna working at the frequency band 5470–5850 MHz, with 19 dBi gain, 16° horizontal and 16° vertical beam widths. In order to avoid possible damage in the measurements, the transmitting system is attached to a pylon located on land.
2) Receiving system: The receiving system is composed of a broadband antenna, an amplifier, and a spectrum analyzer, located on a standard subway train. The receiving antenna is an R&S HL050 Log-Periodic WB antenna, with 8.5 dBi gain, 85° horizontal and 70° vertical beam widths, located in the front car of the train (see Figs. 1 and 2). A Celwritek csa-936327 (teledyne) amplifier working at the frequency band 500–6000 MHz is used to amplify the received power. An Agilent N9912A spectrum analyzer is employed to send the captured received signal power to a laptop, stored for the later processing.

The measurements are conducted in all the cases. In each case, three carrier frequencies—920 MHz, 2400 MHz, and 5705 MHz—are tested to get the influence of the frequency. In order to observe the impact of the antenna polarization,

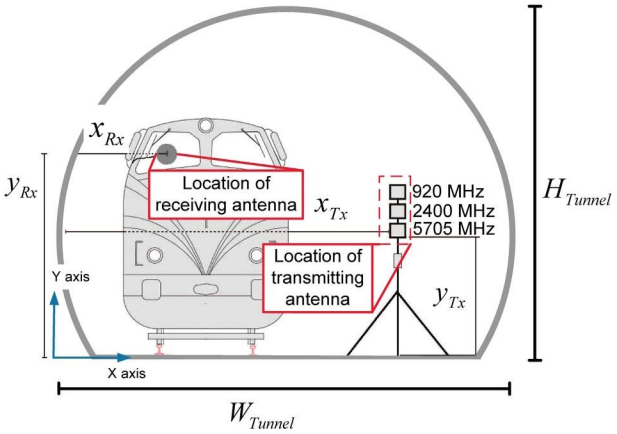

Fig. 2. Front view of the measurement setup in the arched "Type II" tunnel.

both vertical polarization (V-pol.) and horizontal polarization (H-pol.) are measured in the arched "Type I" tunnel. In the arched "Type II" tunnel, the antennas are set to be horizontal polarization. The sampling intervals are shorter than one wavelength, and repeated measurements are taken to collect sufficient samples for study of the fading behavior. Since this study focuses on the large-scale fading property specified in real curved arched tunnels, the small-scale fading is separated from the received power by averaging samples at intervals of 40 wavelengths [46]. The lowest average signal-to-noise-ratio (SNR) measured at a particular location is approximately 30 dB. At most locations, SNR is larger than 30 dB so that an accurate estimation of channel parameters is possible.

B. Measurement Environment

The measurements are carried out in two types of arched curved tunnels of Madrid's subway. As shown in Figs. 1 and 2, there are two types of arched tunnels in the modern subway systems. In order to keep coherence to our previous publications, such as [27], [47], these two types of tunnels are still named Arched "Type I" tunnel and Arched "Type II" tunnel, respectively. "Type I" consists of three plane walls and an arched roof; "Type II" includes arched walls and roof, but a plane floor, more like a semicircle. The arched "Type I" tunnel is more common in the subway tunnels built in the 1980s and 1990s, whereas the arched "Type II" tunnel is more usual in the newly built subway lines, because of the widespread use of the shield machines in the constructions of modern tunnels. Relative position and configuration of the transmission system and receiving system along the train route inside two types of arched tunnels with dimensions 7.59 m × 5.52 m ("Type I" tunnel) and 8.41 m × 6.87 m ("Type II") are illustrated in Figs. 1 and 2 as well. Positions of Tx and Rx as well as the radii of curvature in these two types of tunnels are given by Table I. Three carrier frequencies—920 MHz, 2400 MHz, and 5705 MHz—are used in every case of the measurements. In the curved arched "Type I" tunnel with 500 m radius of curvature, all the measurements are conducted with horizontal and vertical polarizations, respectively. In the curved arched "Type II" tunnel, two radii of curvature (300 m and 500 m) are tested at the three frequencies with horizontal polarization.

III. Measurement Results and Parameter Extraction

A. Received Power in the Curved Arched Tunnels

The received power in all the measurement campaigns are shown in Figs. 3 and 4, respectively. By analyzing these figures, some preliminary observations on the influences of the following factors could be summarized:

1) Frequency: when the other factors (polarization, tunnel, radius of curvature) are the same, wave propagation at the three measured frequencies suffers similar loss. In the straight tunnel, the waveguide theory points out that the wave at higher frequencies experiences the smaller propagation loss. Hence, the fact that the total losses at various frequencies are similar in the measurements, virtually implies that the higher frequencies are more sensitive to the tunnel curve. In terms of the fading, the case in the curved tunnel follows the same law in the straight tunnel: higher frequencies have more severe fading.
2) Polarization: from each sub-figure of Fig. 3 [particularly Fig. 3(a) and (c)], it can be seen that the horizontal polarized wave suffers certain larger propagation loss than the vertical polarized wave in the curved tunnel. This implies that compared with the vertical polarization, the horizontal polarization is much more sensitive to the tunnel curve. Since the width of the measured arched "Type I" tunnel is larger than its height, by employing the modal analysis, the propagation loss of horizontal polarization should be smaller than that of the vertical polarization if the tunnel was straight. But, the final total propagation loss in the real curved tunnel for the horizontal polarization is larger than that of the vertical polarization. This reflects that the excess loss for the horizontal polarization resulting from the tunnel curve could be larger than that for the vertical polarization.
3) Tunnel type: the wave of horizontal polarization at the same frequencies experiences smaller loss in the curved arched "Type I" tunnel than that in the arched "Type II" tunnel. This may come from the fact that the attenuation constant of corresponding modes in the rectangular tunnel (close to the arched "Type I" tunnel) is smaller than that in the circular tunnel (close to the arched "Type II" tunnel).
4) Radius of curvature: in the arched "Type II" tunnel with horizontal polarization, the wave suffers larger propagation loss with the 300 m radius of curvature than that of the 500 m radius of curvature. This follows the common sense that the sharper curve leads to larger propagation loss. Similar results are reported by [11], [34], [37], [40].

These observations justify the measurement data, and implies the factors behind the propagation loss in the curved tunnels as well.

B. Path Loss Exponent and Shadow Fading Extraction

In the log-distance path loss model, the change of the path loss along with the distance is depicted by the path loss

TABLE I
POSITIONS OF TX AND RX IN THE MEASUREMENTS

Tunnel	W_{Tunnel} (m)	H_{Tunnel} (m)	x_{Tx} (m)	y_{Tx} (m)	x_{Rx} (m)	y_{Rx} (m)	Radius of Curvature (m)
"Type I"	7.59	5.52	5.6	2.18	1.1	3	500
"Type II"	8.41	6.87	6.75	2.15	1.7	2.84	300 and 500

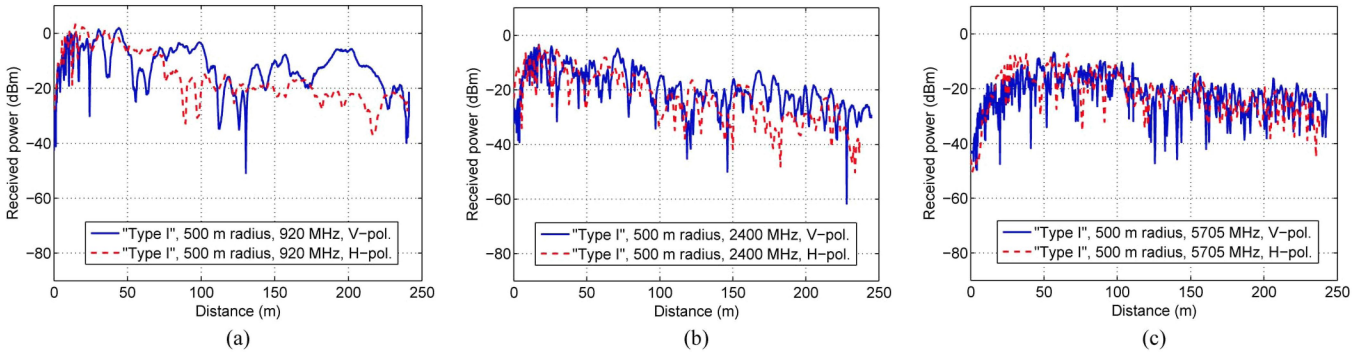

Fig. 3. Measured received power (without small-scale fading) in the traditional curved arched "Type I" tunnel with 500 m radius of curvature with both polarizations at (a) 920 MHz, (b) 2400 MHz, and (c) 5705 MHz.

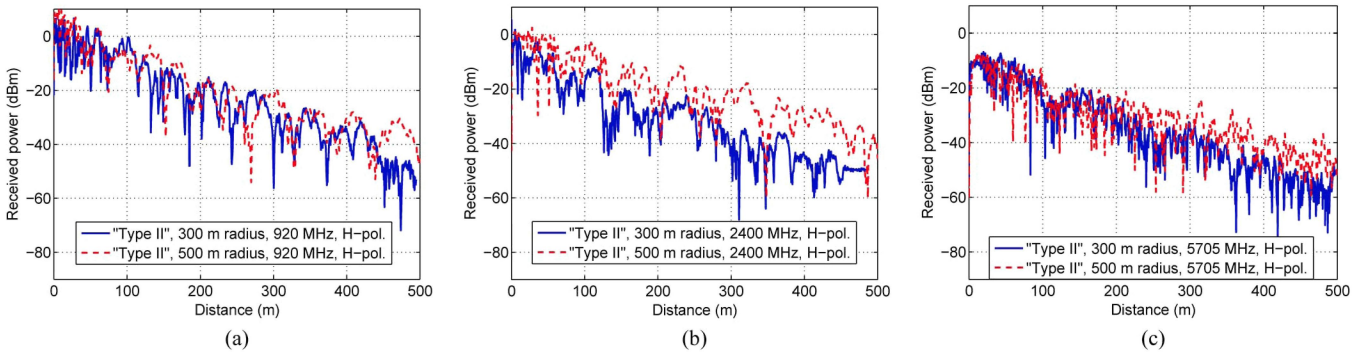

Fig. 4. Measured received power (without small-scale fading) in the modern curved arched "Type II" tunnels with 300 m and 500 m radii of curvature with horizontal polarization at (a) 920 MHz, (b) 2400 MHz, and (c) 5705 MHz.

exponent. Such exponent and shadow fading are extracted from the measured results by using the following expression:

$$L(d) = \overline{L}(d_0) + 10n \lg\left(\frac{d}{d_0}\right) + X_\sigma \qquad (1)$$

where d is the distance (along the track of the tunnel) between Tx and Rx. $L(d)$ is the propagation loss (small-scale fading already filtered out). d_0 is the referenced distance. $\overline{L}(d_0)$ is the media path loss at d_0. n is the path loss exponent. X_σ is the shadow fading. By using the least-square criterion, the path loss exponent n can be received. Fig. 5 gives an example of the least-square fitting of n in the arched "Type I" tunnel at 5705 MHz with horizontal polarization. The shadow fading values can be calculated by using a simple minus to the formula offered above.

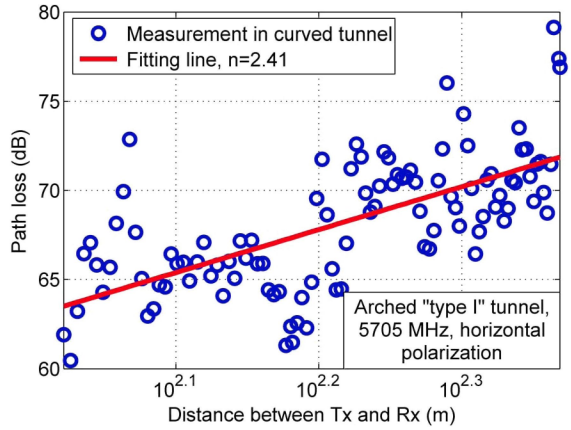

Fig. 5. Path loss and least-square fitting in the arched "Type I" tunnel at 5705 MHz with horizontal polarization.

C. Amplitude Distribution of Shadow Fading

In extensive literature, the log-normal distribution has been empirically confirmed for fitting the amplitude distribution of shadow fading. In this study, the shadow fading is well fitted by the log-normal distribution as well, by passing Kolmogorov-Smirnov, Anderson-Darling, and Chi-Squared tests in Easy Fit [48]. The shadow fading standard deviations (σ) based on the averaging of repeated measurements are given by Tables II and III. Fig. 6 illustrates probability density (PDF) of shadow fading in the arched "Type I" tunnel at 5705 MHz with horizontal polarization.

TABLE II
PATH LOSS EXPONENT AND SHADOW FADING IN THE CURVED ARCHED "TYPE I" TUNNEL

Tunnel:	Arched "Type I";		Radius of Curvature:		500 m	
Frequency	920 MHz		2400 MHz		5705 MHz	
Polarization	Vertical	Horizontal	Vertical	Horizontal	Vertical	Horizontal
Path Loss Exponent	0.94	2.44	1.81	3.73	2.20	2.41
Shadow Fading	Log-Normal Distribution					
Std	4.95 dB	2.18 dB	3.61 dB	4.12 dB	3.36 dB	2.74 dB

TABLE III
PATH LOSS EXPONENT AND SHADOW FADING IN THE CURVED ARCHED "TYPE II" TUNNEL

Tunnel:	Arched "Type II";			Polarization:		Horizontal
Radius of Curvature	500 m			300 m		
Frequency	920 MHz	2400 MHz	5705 MHz	920 MHz	2400 MHz	5705 MHz
Path Loss Exponent	3.36	5.37	4.94	4.61	5.50	4.78
Shadow Fading	Log-Normal Distribution					
Std	6.52 dB	4.67 dB	4.46 dB	4.64 dB	4.09 dB	5.18 dB

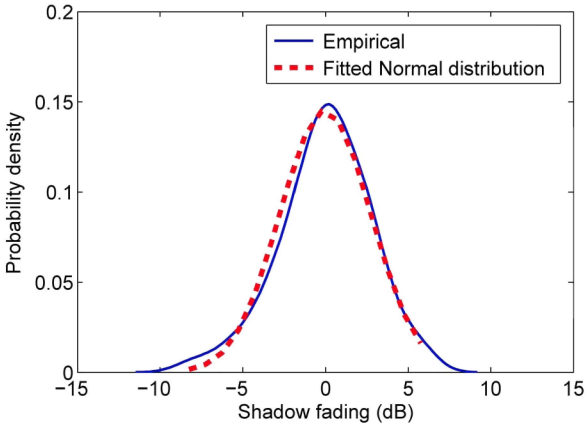

Fig. 6. Probability density of shadow fading in the arched "Type I" tunnel at 5705 MHz with horizontal polarization.

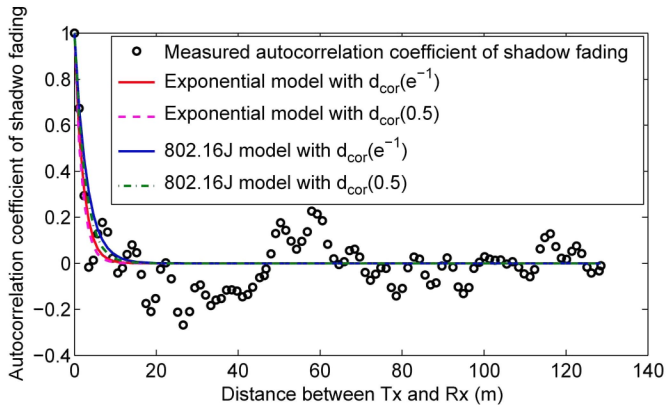

Fig. 7. Measurement result and theoretical results by using least squares (LS) fitting of the autocorrelation coefficient of shadow fading in the arched "Type I" tunnel at 2400 MHz with horizontal polarization.

D. Autocorrelation Calculation and Modeling

Besides the distribution, one of the most important characteristics of the shadow fading is the autocorrelation. Autocorrelation of shadow fading is of interest for power control and base station (or access point) location designing. It is defined as the correlation of shadow fading in different positions of the signal from the same Tx. The autocorrelation is described by the correlation coefficient in numerical documents, such as the Spatial Channel Model (SCM) [49], 802.16J [50], M.2135 [51], etc. The definition is as follows:

$$\rho_{1,2} = \frac{\mathrm{E}\left\{S(d_1)S(d_2)\right\}}{\sigma(d_1)\sigma(d_2)} \tag{2}$$

where $S(d_1)$ is the value of shadow fading in the position with distance d_1; $S(d_2)$ is the value of shadow fading in the position with distance d_2. $\sigma(d_1)$ and $\sigma(d_2)$ are the standard deviations of the shadow fading in the positions with distance d_1 and d_2, respectively.

There are two models widely used for describing the autocorrelation coefficient—the exponential model and 802.16J model. The former is firstly proposed by [52], and then is accepted by the standard [53], [54]. The latter is presented in the standard IEEE 802.16J, which is commercialized user the name "Worldwide Interoperability for Microwave Access (WiMAX)." These two models are with the same structures and there is only one coefficient $\ln 2$ difference. The exponential shadow fading autocorrelation model is expressed below

$$\rho_{\exp}(\Delta d) = e^{(-|\Delta d|/d_{cor})}. \tag{3}$$

The 802.16J model is given as following:

$$\rho_{802.16J}(\Delta d) = e^{(-|\Delta d|/d_{cor})\ln 2} \tag{4}$$

where Δd is the distance between the two observed positions. d_{cor} is the decorrelation distance. There are mainly two definitions for such decorrelation distance. The first one—$d_{cor}(0.5)$—is defined as the distance that the correlation is equal to 0.5 [49]–[51]. The other definition—$d_{cor}(e^{-1})$—is the distance when the correlation is equal to e^{-1} [52]. In order to provide a general reference, both models of autocorrelation coefficient using both definitions of decorrelation distance are calculated by using least squares (LS) fitting based on the repeated measurement results. Fig. 7 demonstrates the measurement result and theoretical results by using least squares (LS) fitting of the autocorrelation coefficient of shadow fading in the arched "Type I" tunnel at 2400 MHz with horizontal polarization.

1) Cross-Correlation Calculation: In order to provide a deep comprehension of the large-scale fading, the cross-correlation is extracted from the measurement results as well. This study is of interested in designing handover algorithms, evaluating performances of macro-diversity schemes, and controlling interference power [55].

The shadow fading cross-correlation coefficient ρ is defined as the cross-correlation coefficient between shadow fading components of two sets of received signals, by using the following expression:

$$\rho = \frac{\sum_{i=1}^{n}(X_i - \overline{X})(Y_i - \overline{Y})}{\sqrt{\sum_{i=1}^{n}(X_i - \overline{X})^2}\sqrt{\sum_{i=1}^{n}(Y_i - \overline{Y})^2}} \quad (5)$$

where X_i and Y_i denote the shadow fading components of two separate received power, $\overline{X}$ and $\overline{Y}$ are the mean of shadow fading components, n is the number of the shadow fading component samples. In this study, n ranges from 200 to 400 in different measurement routes. Usually, if the absolute value of the estimated correlation coefficient lies in [0, 0.1], two random variables can be treated as uncorrelated. In this study, the cross-correlation coefficients of shadow fading between different frequencies, types of tunnels, and polarizations are evaluated from the measurement results.

IV. Large-Scale Fading Characteristics and Analysis

Based on the parameter extraction from the measurement results, the large-scale fading characteristics of wave propagation in curved arched tunnels are quantitatively analyzed and discussed in this section.

A. Path Loss Exponent and Shadow Fading Distribution in Curved Arched Tunnels

Tables II and III show the path loss exponents as well as shadow fading distributions and standard deviations (Std) in the curved arched "Type I" and "Type II" tunnels with various frequencies, radii of curvature, and polarizations, respectively. Following findings can be summarized:

1) Path loss exponents in the curved arched "Type II" tunnel are from 3.36 to 5.50, larger than the values of the corresponding cases in the curved arched "Type I" tunnel, which are from 0.94 to 3.73. This reflects the fact that even though the arched "Type II" tunnel is more welcome in the newly built subway lines constructed by the shield machines, the wave propagation suffers larger loss than that in the traditional arched "Type I" tunnel.
2) Most of the path loss exponents are larger than 2 (which equals the case of free-space propagation), and much larger than the cases of the straight tunnels where the waveguide effect is established. This implies that the tunnel curve reduces the waveguide effect, and leads to the excess loss of propagation compared to the cases of the straight tunnels.
3) In Table III, the path loss exponents of the horizontal polarized wave propagation in the arched "Type II" tunnel with 300 m radius of curvature are between 4.61 and 5.50, which are larger than the values (3.36–5.37) with 500 m radius of curvature. This implies that the sharper the tunnel curve is, the larger the path loss is. Similar conclusions can be found in [39].
4) No matter which type of the tunnel is, the path loss exponents at higher frequencies are slightly larger than those at lower frequencies. Given the fact that the higher frequencies experience smaller path loss in the straight tunnels, it could be concluded that the higher frequencies are more sensitive to the tunnel curve. An even more extreme case is presented by [56], in which the path loss could even increase along with the increase of frequency in curved tunnels.
5) The path loss exponents of the horizontal polarized wave at various frequencies are from 2.41 to 3.73, which are 8.71%–61.48% larger than those values (0.94–2.20) of the vertical polarized wave in the arched "Type I" tunnel with 500 m radius of curvature. This indicates that the excess loss for the horizontal polarization resulting from the tunnel curve is larger than that for the vertical polarization, because the original propagation loss of horizontal polarization should be smaller in the measured tunnel (whose width is larger than its height) if it was straight.
6) The standard deviations of the log-normal distributed shadow fading are from 2.18 dB to 4.95 dB in the curved arched "Type I" tunnel, and are from 4.09 dB to 6.52 dB in the curved arched "Type II" tunnel. These values are larger than the standard deviations of the shadow fading in the other railway scenarios, such as train station, cutting, and viaduct.

B. Integration and Comparison of the Path Loss Exponent and Shadow Fading Distribution of the Curved Arched Tunnel

The path loss exponent and shadow fading in various tunnels between 900 MHz and 5.7 GHz bands are summarized in Table IV, where LOS and NLOS denote line-of-sight and non-line-of-sight, respectively. It can be found that no matter of which type, the straight tunnel always leads to smaller path loss exponents than the corresponding curved tunnel. In the straight tunnels, the path loss exponent and standard deviation of shadow fading in the road tunnel is smaller than the railway tunnel, whereas the subway tunnel gets the worst propagation condition. This is because that the dimensions of the road tunnel are usually larger than the railway tunnel, and the subway tunnel usually is the smallest type. The same observation can be found in the curved tunnel groups as well. Table IV is helpful to give a comprehensive insight into the propagation characteristics and corresponding engineering suggestions inside various tunnels. For instance, the access points or the transmitters of ITS should be deployed more densely in the railway tunnel than the road tunnel; more relays should be used in the network planning in the subway tunnels.

A complete table (Table V) is made to provide the path loss exponent and shadow fading distribution of the curved arched tunnel scenario, the train station scenario, the crossing bridge scenario, the cutting scenario, and the viaduct scenario. By filling the gap of the knowledge of the curved arched tunnel

TABLE IV
PATH LOSS EXPONENT AND SHADOW FADING DISTRIBUTION COMPARISON AMONG VARIOUS TUNNELS

Tunnel type	Frequency [MHz]	Path loss exponent	Shadow fading Std [dB]	Radius of curvature [m]
Curved subway tunnel	920	0.94-2.44	2.18-4.95	500
"Type I"	2400	1.81-3.73	3.61-4.12	500
Arched	5705	2.20-2.41	2.74-3.36	500
Curved subway tunnel	920	3.36-4.61	4.64-6.52	300-500
"Type II"	2400	5.37-5.50	4.09-4.67	300-500
Arched	5705	4.78-4.94	4.46-5.18	300-500
Curved railway tunnel	954-	0.55-2.97	4.87-5.00	4500-5800
"Type I" Arched [57]	2000			
Curved subway tunnel	2400	Wide: 5.49	2.75	400
"Type I" Arched [19]	5000	Narrow: 7.13	4.17	400
Straight road tunnel	2800-	0.57-0.82	2.70	–
"Type II" Arched [58]	5000			
Straight railway tunnel	954-	1.40-2.03	4.36-4.95	–
"Type I" Arched [57], [59]	2000			
Straight subway tunnel	945-	LOS: 1.65-1.94	3.40-4.60	–
Rectangular [60]–[62]	2650	NLOS: 3.20-7.28	5.47	–

TABLE V
PATH LOSS EXPONENT AND SHADOW FADING DISTRIBUTION OF THE MAIN PROPAGATION SCENARIOS OF RAIL TRAFFIC

Rail traffic scenario	Frequency [MHz]	Path loss exponent	Shadow fading Std [dB]	Remark
Curved arched	920	0.94-2.44	2.18-4.95	Radius of
tunnel "Type I"	2400	1.81-3.73	3.61-4.12	curvature:
	5705	2.20-2.41	2.74-3.36	500 m
Curved arched	920	3.36-4.61	4.64-6.52	Radius of
tunnel "Type II"	2400	5.37-5.50	4.09-4.67	curvature:
	5705	4.78-4.94	4.46-5.18	300-500 m
Train station [63], [64]	930	Extended Hata	1.57-	Excess loss [dB]:
			3.92	0.37-21.80
Crossing bridge [65], [66]	930	Extended Hata	1.88-	Excess loss [dB]:
			4.73	5.96-14.18
Cutting [67]	930	Deep: $13.05e^{-0.039(w_{up}-w_{down})}$	2.10-	w_{up}: upper width
		Low: $1.66{w_{down}}^2 - 58.51w_{down} + 517.6$	4.50	w_{down}: lower width
Viaduct [68], [69]	930	$2.36 - 0.43H$, $d \leq 400$ m	2.00-	H: viaduct height
		$16.5 - 0.2H$, $d > 400$ m	2.32	d: distance

scenario, Table V could be helpful to establish a comprehensive understanding of the large-scale fading characteristics in the main propagation scenarios of rail traffic. In general, the path loss exponent in the curved arched tunnel is obviously larger than that of the other rail traffic scenarios. This is because that the tunnel curve leads to the excess loss, so that the path loss exponent increases. The shadow fading standard deviation in the curved arched tunnel is larger than that of the train station and viaduct scenarios, but relatively closer to the crossing bridge and cutting scenarios. This implies that the shadow fading in the curved tunnel comes from the extensive reflected, scattered and diffracted waves generated by the curved tunnel route and walls, like the steep walls on both sides of the track in the crossing bridge and cutting scenarios.

In order to show the difference of the channel in the curved arched tunnel scenario from other "typical" scenarios, ten standard scenarios in the WINNER model [54] are referred. Table VI gives the comparisons of path loss exponent and standard deviation of shadow fading. It can be found that most of the path loss exponents in the curved tunnel scenario are larger than that of the standard scenarios in WINNER. Moreover, the standard deviations of shadow fading in the curved tunnel scenario are usually between the values in the outdoor and indoor scenarios of WINNER. Thus, the already existing scenarios cannot represent the characteristics of large-scale fading in the real curved tunnels. Given the safety critical requirements of the ITS communication systems, the propagation characterization presented in this paper is still recommended to be used for the network planning and system design of the curved tunnel scenario.

C. Autocorrelation Characteristics of Shadow Fading in Curved Arched Tunnels

Tables VII and VIII give the statistics of the decorrelation distances in the curved arched "Type I" and "Type II" tunnels with two definitions of the decorrelation distances, various frequencies, radii of curvature, and polarizations, respectively. The decorrelation distances defined as $d_{cor}(0.5)$ are shorter than the values of the definition of $d_{cor}(e^{-1})$. The mean values of decorrelation distances in the arched "Type I" tunnel with the 500 m radius of curvature are 1.86–4.10 m, 2.26–3.43 m, and 1.79–3.28 m, at 920 MHz, 2400 MHz, and 5705 MHz, respectively. In the arched "Type II" tunnel, when the radius of curvature is 500 m, the mean values of decorrelation distances

TABLE VI
COMPARISONS OF LARGE-SCALE FADING CHARACTERISTICS BETWEEN CURVED ARCHED TUNNEL SCENARIO AND STANDARD SCENARIOS IN WINNER [54]

Propagation scenario			Frequency [GHz]	Path loss exponent	Shadow fading Std [dB]	Remark
Arched tunnel	"Type I"	Curved	0.92	0.94-2.44	2.18-4.95	Radius of
			2.4	1.81-3.73	3.61-4.12	curvature:
			5.705	2.20-2.41	2.74-3.36	500 m
Arched tunnel	"Type II"	Curved	0.92	3.36-4.61	4.64-6.52	Radius of
			2.4	5.37-5.50	4.09-4.67	curvature:
			5.705	4.78-4.94	4.46-5.18	300-500 m
Indoor Office/	A1	LOS	2-6	1.87	3.00	
Residential		NLOS	2-6	3.68/2.00	4.00	
Indoor to Outdoor/ Outdoor to Indoor	A2/B4/C4	NLOS	2-6	2.27	7.00	
Typical Urban	B1	LOS	2-6	2.27/4.00	3.00	
Micro-cell		NLOS	2-6	$\max(2.8-0.0024d_k, 1.84)$	4.00	$d_k \leq 400$ m
Large Indoor	B3	LOS	2-6	1.39	3.00	
Hall		NLOS	2-6	3.78	4.00	
Suburban	C1	LOS	2-6	2.38/4.00	4.00/6.00	
		NLOS	2-6	$(4.49-0.655\lg(h_{BS}))$	8.00	$h_{BS}=25$ m
Typical Urban	C2	LOS	2-6	2.60/4.00	4.00/6.00	
Macro-Cell		NLOS	2-6	$(4.49-0.655\lg(h_{BS}))$	8.00	$h_{BS}=25$ m
Rural	D1	LOS	2-6	2.15/4.00	4.00/6.00	
Macro-Cell		NLOS	2-6	2.51	8.00	
Moving Networks BS-MRS, Rural	D2a	LOS	2-6	2.15/4.00	4.00	

TABLE VII
DECORRELATION DISTANCE STATISTIC IN THE CURVED ARCHED "TYPE I" TUNNEL

Tunnel:	Arched "Type I";								Radius of Curvature:		500 m	
Frequency	920 MHz				2400 MHz				5705 MHz			
Polarization	Vertical		Horizontal		Vertical		Horizontal		Vertical		Horizontal	
Decorrelation Distance [m]	d (0.5)	d (e^{-1})	d (0.5)	d (e^{-1})	d (0.5)	d (e^{-1})	d (0.5)	d (e^{-1})	d (0.5)	d (e^{-1})	d (0.5)	d (e^{-1})
10%	2.47	3.12	1.51	1.51	1.66	1.95	1.96	1.96	0.89	1.18	0	1.18
50%	3.39	4.19	2.04	2.04	2.24	2.82	1.96	3.23	1.45	2.02	1.18	1.18
90%	4.19	4.81	2.04	3.51	3.11	4.21	3.23	3.23	3.18	6.64	3.49	3.49
Mean	3.27	4.10	1.86	2.62	2.26	3.43	2.46	3.16	1.89	3.28	1.79	2.08

TABLE VIII
DECORRELATION DISTANCE STATISTIC IN THE CURVED ARCHED "TYPE II" TUNNEL

Tunnel:	Arched "Type II";								Polarization:		Horizontal	
Radius of Curvature	300 m						500 m					
Frequency	920 MHz		2400 MHz		5705 MHz		920 MHz		2400 MHz		5705 MHz	
Decorrelation Distance [m]	d (0.5)	d (e^{-1})	d (0.5)	d (e^{-1})	d (0.5)	d (e^{-1})	d (0.5)	d (e^{-1})	d (0.5)	d (e^{-1})	d (0.5)	d (e^{-1})
10%	3.89	5.30	1.59	1.86	2.96	2.96	9.83	10.50	0.73	0.73	2.96	4.00
50%	5.74	6.67	1.86	2.33	2.96	3.44	10.50	11.38	0.73	2.66	4.00	4.84
90%	8.79	11.50	2.80	3.30	3.44	9.18	11.08	37.77	2.66	2.66	4.84	6.60
Mean	6.35	8.87	2.05	2.56	3.23	5.50	11.19	16.75	1.41	1.83	4.13	5.78

are 11.19–16.75 m, 1.41–1.83 m, and 4.13–5.78 m, at 920 MHz, 2400 MHz, and 5705 MHz, respectively. Most of these values are larger than the corresponding values when the radius of curvature is 300 m. This implies that the sharper curve favors the decorrelation of the received signal. The decorrelation distances in the curved tunnel are much shorter than those in the urban macro environments (32 m, 45 m, and 97 m) [70] as well as other outdoor rail traffic scenarios, such as viaduct (14.81–131.6 m) [54], [71], [72]. This indicates that compared with the open space, the shadow fading component along the distance varies considerably faster in the curved confined space, e.g., the curved subway tunnels in this study. This means that the propagation inside curved tunnels needs special attention for communication system design.

The mean error (ME), standard deviation (Std) and root mean square error (RMSE) between all the measurement results and the two models with two definitions are utilized to evaluate the fitness. The results are summarized in Table IX. Generally speaking, both models fit the measurement shadow fading auto-correlation well, because the mean ME are close to 0, and the

TABLE IX
STATISTIC VALUES OF THE ME, STD, AND RMSE BETWEEN MEASUREMENTS AND THE EXPONENTIAL MODEL AND THE 802.16J MODEL

Tunnel:		Arched "Type I"				Arched "Type II"			
Autocorrelation Model		Exponential Model		802.16J Model		Exponential Model		802.16J Model	
Decorrelation Distance		d (0.5)	d (e^{-1})	d (0.5)	d (e^{-1})	d (0.5)	d (e^{-1})	d (0.5)	d (e^{-1})
ME	10%	0.016	0.018	0.022	0.027	0.024	0.030	0.033	0.043
	50%	0.012	0.017	0.018	0.025	0.013	0.022	0.021	0.032
	90%	0.007	0.012	0.010	0.018	0.005	0.006	0.007	0.009
	Mean	0.012	0.016	0.017	0.024	0.012	0.017	0.017	0.024
Std	10%	0.100	0.096	0.100	0.091	0.101	0.094	0.092	0.086
	50%	0.148	0.140	0.141	0.134	0.107	0.104	0.103	0.100
	90%	0.237	0.230	0.224	0.217	0.280	0.271	0.267	0.256
	Mean	0.158	0.016	0.150	0.144	0.147	0.140	0.138	0.131
RMSE	10%	0.101	0.097	0.100	0.093	0.101	0.095	0.092	0.087
	50%	0.148	0.141	0.142	0.136	0.107	0.104	0.104	0.101
	90%	0.237	0.230	0.225	0.219	0.281	0.272	0.268	0.260
	Mean	0.158	0.151	0.151	0.146	0.148	0.140	0.140	0.133

TABLE X
CROSS-CORRELATION OF THE SHADOW FADING BETWEEN THE 920 MHZ, 2400 MHZ, AND 5705 MHZ IN CURVED SUBWAY TUNNELS

Tunnel:	Arched "Type I"		Radius: 500 m
Frequency Bands	920 MHz vs 2400 MHz	980 MHz vs 5705 MHz	2400 MHz vs 5705 MHz
Vertical Polarization	0.41	0.24	0.08
Horizontal Polarization	0.24	0.13	0.08
Tunnel:	Arched "Type II"		Polarization: Horizontal
Frequency Bands	920 MHz vs 2400 MHz	980 MHz vs 5705 MHz	2400 MHz vs 5705 MHz
Radius: 300 m	0.23	0.12	0.04
Radius: 500 m	0.27	0.04	0.07
Tunnel: Arched "Type I"	Tunnel: Arched "Type II"	Radius: 500 m	Polarization: Horizontal
Frequency Bands	920 MHz	2400 MHz	5705 MHz
Type I vs Type II	0.05	0.05	0.04

mean RMSE are between 0.140 and 0.158. However, by comparison between the two models, the mean RMSE of the exponential model is slightly larger than the 802.16J model, which means that the 802.16J model is a more suitable model for the measurement data in real curved arched subway tunnels. No matter in which type of tunnel and model, the fitness of using the decorrelation distance definition $d_{cor}(e^{-1})$ is better than $d_{cor}(0.5)$.

D. Cross-Correlation Characteristics of Shadow Fading in Curved Arched Tunnels

Cross-correlation characteristics of shadow fading in curved tunnels between various measurement configurations are shown in Table X. The shadowing cross-correlation in the sharper curve (300 m radius of curvature) tends to be weaker than that of the gentle curve (500 m radius of curvature), but the difference is not substantial. It implies that the variation of curved radius in the tunnel has little impact on shadowing cross-correlation. Moreover, the cross-correlation coefficients between various frequencies and different types of tunnels are smaller than 0.41. This means that the signals in different frequencies or types of tunnels are uncorrelated. The reasons of such a uncorrelation (or low correlation) are analyzed by [1] in detail, so they are not discussed here again.

Based on the above results, frequency diversity between the three bands (920 MHz, 2400 MHz, and 5705 MHz) holds promise for diversity gains since the channel effects in these three bands are essentially uncorrelated. In other words, various communication systems at 900 MHz frequency band (GSM/GSM-R/LTE/TETRA/LTE-R), 2.4 GHz frequency band (Wi-Fi/UMTS/LTE/CBTC/LTE-R), and 5.8 GHz (CBTC, custom systems, etc), are promising to work together in the same curved tunnel without severe interference. On the other hand, the fact that the channels at the same frequency in different types of curved tunnels are uncorrelated, indicates that the type of tunnel can significantly affect the shadow fading of received signal. Hence, it is suggested that the network planning in different types of curved arched tunnels should be conducted independently.

V. DISCUSSIONS

Based on the large-scale fading characteristics and analysis offered above, the following discussions can be made:

1) Path loss: it is found that the path loss exponents in the "Type II"—3.36 to 5.50—are larger than the values in the "Type I" tunnel—0.94 to 3.73. This implies that the transmitters (access points) can be deployed more sparsely in the curved traditional arched "Type I" tunnels than in the modern "Type II" tunnels. The fact that most of the path loss exponents are larger than 2, reflects that the tunnel curve indeed reduces the waveguide effect, so that the wave propagation suffers much larger loss than the cases of the straight tunnels. Meanwhile, the measurement results indicates that the sharper the tunnel curve is, the

larger the path loss is. Moreover, it is found that both the horizontal polarization and the higher frequencies are more sensitive to the tunnel curve.

2) Shadow fading distribution: the measured shadow fading can be well fitted by the log-normal distribution, with the standard deviations from 2.18 dB to 4.95 dB in the curved arched "Type I" tunnel, and 4.09 dB to 6.52 dB in the curved arched "Type II" tunnel. This means that the wave propagation in curved subway tunnels experiences more severe shadow fading than the other railway scenarios, such as train station, cutting, and viaduct.
3) Compared with the standard scenarios of WINNER, most of the path loss exponents in the curved tunnel scenario are larger than that of the standard scenarios. Furthermore, the standard deviations of shadow fading in the curved tunnel scenario are usually between the values in the outdoor and indoor scenarios of WINNER. Thus, it is not suggested to use the existing scenarios to represent the curved tunnel. The propagation characterization presented in this study could be employed for the network planning and system design of the curved tunnel scenario.
4) Autocorrelation and decorrelation distance: he mean values of decorrelation distances are several meters, much shorter than those in the urban macro environments or other outdoor rail traffic scenarios. This indicates that compared with the open space, the shadow fading component along the distance varies considerably faster in the curved confined space, and therefore, the propagation inside curved tunnels needs special attention for communication system design. In terms of the autocorrelation model, the 802.16J model is a more suitable model for the measurement data in real curved arched subway tunnels.
5) Cross-correlation of shadow fading: the signals in different frequencies or types of tunnels are uncorrelated. This gives the chance to employ the frequency diversity to ensure reliable communication in subway systems for emergency cases. Moreover, various communication systems at various frequency bands are expected to work simultaneously in the same curved tunnel without severe interference. Since the type of tunnel significantly affects the shadow fading of received signal, the network planning in different types of curved arched tunnels should be conducted independently.

VI. Conclusion

A set of comprehensive propagation measurements are conducted in the curved traditional arched "Type I" and modern arched "Type II" subway tunnels with 300 m and 500 m radii of curvature, horizontal and vertical polarizations, at 920 MHz, 2400 MHz, and 5705 MHz, respectively. The extensive measurements provides the insight into the large-scale fading characteristics in real curved subway tunnels at various frequencies. The qualitative analysis and corresponding findings are useful for the link budget, channel modeling, and validation for simulators of various wireless communication systems deployed in real curved tunnels, realizing the intelligent transportation system in subway and railway systems.

References

[1] B. Zhang, Z. Zhong, K. Guan, R. He, and C. Briso, "Shadow fading correlation of multi-frequencies in curved subway tunnels," in *Proc. IEEE Conf. ITSC*, Qingdao, China, 2014, pp. 1111–1116.

[2] K. Dar, M. Bakhouya, J. Gaber, M. Wack, and P. Lorenz, "Wireless communication technologies for ITS applications [topics in automotive networking]," *IEEE Commun. Mag.*, vol. 48, no. 5, pp. 156–162, May 2010.

[3] H. Wang, F. Yu, L. Zhu, T. Tang, and B. Ning, "Finite-state Markov modeling for wireless channels in tunnel communication-based train control systems," *IEEE Trans. Intell. Transp. Syst.*, vol. 15, no. 3, pp. 1083–1090, Jun. 2014.

[4] X. Cheng *et al.*, "Electrified vehicles and the smart grid: The its perspective," *IEEE Trans. Intell. Transp. Syst.*, vol. 15, no. 4, pp. 1388–1404, Aug. 2014.

[5] X. Cheng *et al.*, "Cooperative mimo channel modeling and multi-link spatial correlation properties," *IEEE J. Sel. Areas Commun.*, vol. 30, no. 2, pp. 388–396, Feb. 2012.

[6] GSM-R Specifications. [Online]. Available: http://www.uic.asso.fr

[7] *Terrestrial Trunked Radio (TETRA); Voice Plus Data (V+D); Designers' Guide; Part 3: Direct Mode Operation (DMO)*, ETSI, Sophia Antipolis, France, 2000.

[8] A. Hrovat, T. Javornik, and G. Kandus, "Adjacent channel interference analyses in tetra direct mode operation," *WSEAS Trans. Commun.*, vol. 7, no. 10, pp. 1055–1065, Oct. 2008.

[9] K. Guan, Z. Zhong, and B. Ai, "Assessment of LTE-R using high speed railway channel model," in *Proc. 3rd Int. Conf. Commun. Mobile Comput.*, Qingdao, China, 2011, pp. 461–464.

[10] *IEEE Standard for Communications-Based Train Control (CBTC) Performance and Functional Requirements*, IEEE Std. 1474.1-1999, Dec. 1999.

[11] E. Masson *et al.*, "Radio wave propagation in curved rectangular tunnels at 5.8 GHz for metro applications," in *Proc. 11th Int. Conf. ITST*, St. Petersburg, Russia, 2011, pp. 81–85.

[12] B. Ai *et al.*, "Challenges toward wireless communications for high-speed railway," *IEEE Trans. Intell. Transp. Syst.*, vol. 15, no. 5, pp. 2143–2158, Oct. 2014.

[13] X. Cheng, C.-X. Wang, B. Ai, and H. Aggoune, "Envelope level crossing rate and average fade duration of non-isotropic vehicle-to-vehicle ricean fading channels," *IEEE Trans. Intell. Transp. Syst.*, vol. 15, no. 1, pp. 62–72, Feb. 2014.

[14] X. Cheng *et al.*, "Wideband channel modeling and ici cancellation for vehicle-to-vehicle communication systems," *IEEE J. Sel. Areas Commun.*, vol. 31, no. 9, pp. 434–448, Sep. 2013.

[15] A. Hrovat *et al.*, "Empirical path loss model and wimax measurements in urban and suburban environment," *WSEAS Trans. Commun.*, vol. 5, no. 8, pp. 1328–1334, Aug. 2006.

[16] D. Dudley, M. Lienard, S. Mahmoud, and P. Degauque, "Wireless propagation in tunnels," *IEEE Antennas Propag. Mag.*, vol. 49, no. 2, pp. 11–26, Apr. 2007.

[17] A. Hrovat, G. Kandus, and T. Javornik, "Four-slope channel model for path loss prediction in tunnels at 400 MHz," *IET Microw. Antennas Propag.*, vol. 4, no. 5, pp. 571–582, May 2010.

[18] C. Briso-Rodriguez, J. Cruz, and J. Alonso, "Measurements and modeling of distributed antenna systems in railway tunnels," *IEEE Trans. Veh. Technol.*, vol. 56, no. 5, pp. 2870–2879, Sep. 2007.

[19] K. Guan, Z. Zhong, J. I. Alonso, and C. Briso, "Measurement of distributed antenna systems at 2.4 GHz in a realistic subway tunnel environment," *IEEE Trans. Veh. Technol.*, vol. 61, no. 2, pp. 834–837, Feb. 2012.

[20] K. Guan, Z. Zhong, B. Ai, and C. Briso, "Propagation mechanism analysis before the break point inside tunnels," in *Proc. IEEE 74th Veh. Technol. Conf.*, San Francisco, CA, USA, 2011, pp. 1–5.

[21] D. Didascalou, T. Schafer, F. Weinmann, and W. Wiesbeck, "Ray-density normalization for ray-optical wave propagation modeling in arbitrarily shaped tunnels," *IEEE Trans. Antennas Propag.*, vol. 48, no. 9, pp. 1316–1325, Sep. 2000.

[22] F. Pallares, F. Juan, and L. Juan-Llacer, "Analysis of path loss and delay spread at 900 MHz and 2.1 GHz while entering tunnels," *IEEE Trans. Veh. Technol.*, vol. 50, no. 3, pp. 767–776, May 2001.

[23] A. V. Popov and N. Y. Zhu, "Modeling radio wave propagation in tunnels with a vectorial parabolic equation," *IEEE Trans. Antennas Propag.*, vol. 48, no. 9, pp. 1403–1412, Sep. 2000.

[24] X. Cheng, C.-X. Wang, D. Laurenson, S. Salous, and A. Vasilakos, "An adaptive geometry-based stochastic model for non-isotropic mimo mobile-to-mobile channels," *IEEE Trans. Wireless Commun.*, vol. 8, no. 9, pp. 4824–4835, Sep. 2009.

[25] Y. Zhang and Y. Hwang, "Characterization of UHF radio propagation channels in tunnel environments for microcellular and personal communications," *IEEE Trans. Veh. Technol.*, vol. 47, no. 1, pp. 283–296, Feb. 1998.

[26] Y. Zhang, "Novel model for propagation loss prediction in tunnels," *IEEE Trans. Veh. Technol.*, vol. 52, no. 5, pp. 1308–1314, Sep. 2003.

[27] K. Guan *et al.*, "Propagation mechanism modeling in the near-region of arbitrary cross-sectional tunnels," *Int. J. Antennas Propag.*, vol. 2012, 2012, Art. ID. 183 145. [Online]. Available: http://dx.doi.org/10.1155/2012/183145

[28] A. Hrovat and T. Javornik, "Analysis of radio propagation models for smart city applications," *Int. J. Commun.*, vol. 7, no. 4, pp. 83–92, 2013.

[29] K. Guan *et al.*, "Complete propagation model in tunnels," *IEEE Antennas Wireless Propag. Lett.*, vol. 12, pp. 741–744, Jul. 2013.

[30] K. Guan, Z. Zhong, B. Ai, R. S. He, and C. Briso, "Five-zone propagation model for large-size vehicles inside tunnels," *Progr. Electromagn. Res.*, vol. 138, pp. 389–405, Jul. 2013.

[31] K. Guan *et al.*, "Complete propagation model structure inside tunnels," *Progr. Electromagn. Res.*, vol. 141, pp. 711–726, Aug. 2013.

[32] D. Didascalou, M. Dottling, T. Zwick, and W. Wiesbeck, "A novel ray-optical approach to model wave propagation in curved tunnels," in *Proc. IEEE VTS 50th Veh. Technol. Conf.*, Amsterdam, The Netherlands, 1999, vol. 4, pp. 2313–2317.

[33] J. S. Lamminmaki and J. J. A. Lempiainen, "Radio propagation characteristics in curved tunnels," *Proc. Inst. Elect. Eng.—Microw. Antennas Propag.*, vol. 145, no. 4, pp. 327–331, Aug. 1998.

[34] M. Lienard, S. Betrencourt, and P. Degauque, "Theoretical and experimental approach of the propagation at 2.5 GHz and 10 GHz in straight and curved tunnels," in *Proc. IEEE 50th VTC—Fall*, 1999, vol. 4, pp. 2268–2271.

[35] X. Cheng *et al.*, "An improved parameter computation method for a MIMO V2V Rayleigh fading channel simulator under non-isotropic scattering environments," *IEEE Commun. Lett.*, vol. 17, no. 2, pp. 265–268, Feb. 2013.

[36] N. Sood, L. Liang, S. V. Hum, and C. D. Sarris, "Ray-tracing based modeling of ultra-wideband pulse propagation in railway tunnels," in *Proc. IEEE Int. Symp. APSURSI*, Spokane, WA, USA, 2011, pp. 2383–2386.

[37] T.-S. Wang and C.-F. Yang, "Simulations and measurements of wave propagations in curved road tunnels for signals from GSM base stations," *IEEE Trans. Antennas Propag.*, vol. 54, no. 9, pp. 2577–2584, Sep. 2006.

[38] X. Cheng, C.-X. Wang, D. Laurenson, S. Salous, and A. Vasilakos, "New deterministic and stochastic simulation models for non-isotropic scattering mobile-to-mobile Rayleigh fading channels," *Wireless Commun. Mobile Comput.*, vol. 11, no. 7, pp. 829–842, Jul. 2011.

[39] Y. Zhang, Y. Hwang, and P. Ching, "Characterization of UHF radio propagation channel in curved tunnels," in *Proc. 7th IEEE Int. Symp. PIMRC*, Taipei, Taiwan, 1996, vol. 3, pp. 798–802.

[40] R. Martelly and R. Janaswamy, "Modeling radio transmission loss in curved, branched and rough-walled tunnels with the ADI-PE method," *IEEE Trans. Antennas Propag.*, vol. 58, no. 6, pp. 2037–2045, Jun. 2010.

[41] P. Bernardi, D. Caratelli, R. Cicchetti, V. Schena, and O. Testa, "A numerical scheme for the solution of the vector parabolic equation governing the radio wave propagation in straight and curved rectangular tunnels," *IEEE Trans. Antennas Propag.*, vol. 57, no. 10, pp. 3249–3257, Oct. 2009.

[42] M. Nilsson, J. Slettenmark, and C. Beckman, "Wave propagation in curved road tunnels," in *Proc. IEEE Antennas Propag. Soc. Int. Symp.*, 1998, vol. 4, pp. 1876–1879.

[43] S. F. Mahmoud, "On modal propagation of high frequency electromagnetic waves in straight and curved tunnels," in *Proc. IEEE Antennas Propag. Soc. Int. Symp.*, 2004, vol. 3, pp. 2963–2966.

[44] A. Hrovat, G. Kandus, and T. Javornik, "A survey of radio propagation modeling for tunnels," *IEEE Commun. Surveys Tuts.*, vol. 16, no. 2, pp. 658–669, 2nd Quart. 2014.

[45] A. Hrovat, G. Kandus, and T. Javornik, "Path loss analyses in tunnels and underground corridors," *Int. J. Commun.*, vol. 6, no. 3, pp. 136–144, Aug. 2012.

[46] W. C. Y. Lee, "Estimate of local average power of a mobile radio signal," *IEEE Trans. Veh. Technol.*, vol. VT-34, no. 1, pp. 22–27, Feb. 1985.

[47] K. Guan, Z. Zhong, B. Ai, and C. Briso, "Modeling of the division point of different propagation mechanisms in the near-region within arched tunnels," *Wireless Pers. Commun.*, vol. 68, no. 3, pp. 489–505, Feb. 2013. [Online]. Available: http://dx.doi.org/10.1007/s11277-011-0464-7

[48] K. Schittkowski, "EASY-FIT: A software system for data fitting in dynamical systems," *Structural and Multidisc. Optim.*, vol. 23, no. 2, pp. 153–169, Mar. 2002.

[49] *Spatial Channel Model for Multiple Input Multiple Output (MIMO) Simulations*, 3GPP TR 25.996 V6.1.0, Sep. 2003. [Online]. Available: http://www.3gpp.org/ftp/Specs/html-info/25996.htm

[50] *Multi-Hop Relay Systemevaluation Methodology (Channel Model and Performance Metrics)*, IEEE802.16j-06/013r3, 2007.

[51] "Guidelines for evaluation of radio interface technologies for IMT-Advanced," ITU-R, Geneva, Switzerland, Tech. Rep. ITU-R M.2135, 2008.

[52] M. Gudmundson, "Correlation model for shadow fading in mobile radio systems," *Electron. Lett.*, vol. 27, no. 23, pp. 2145–2146, Nov. 1991.

[53] "Guidelines for evaluation of radio transmission technologies for IMT-2000," ITU-R, Geneva, Switzerland, Rec.ITU-R M.1225, 1997.

[54] *WINNER II Channel Models*, Deliverable 1.1.2 v.1.2, 2007.

[55] S. Szyszkowicz, H. Yanikomeroglu, and J. Thompson, "On the feasibility of wireless shadowing correlation models," *IEEE Trans. Veh. Technol.*, vol. 59, no. 9, pp. 4222–4236, Nov. 2010.

[56] J. Sun and C. Zhang, "Analysis of transmission characteristics of curved tunnel with arbitrary cross section using hybrid mode matching/finite elements approach," in *Proc. IEEE Int. Symp. Commun. Inf. Technol.*, 2005, vol. 1, pp. 63–66.

[57] "Ningde high-speed railway tunnel covering research report," GCI Science & Technology Co., Ltd., Guangzhou, China, Tech. Rep., 2008.

[58] J. M. Molina-Garcia-Pardo, M. Lienard, and P. Degauque, "Propagation in tunnels: Experimental investigations and channel modeling in a wide frequency band for MIMO applications," *EURASIP J. Wireless Commun. Netw.*, vol. 2009, no. 1, Mar. 2009, Art. ID. 560 571. [Online]. Available: http://jwcn.eurasipjournals.com/content/2009/1/560571

[59] N. Wang, "A uniform path-loss model by Power Balance Theory (PBT) and its application on tunnels," in *Proc. 9th ISAPE*, Nov. 2010, pp. 481–484.

[60] D. Didascalou, J. Maurer, and W. Wiesbeck, "Subway tunnel guided electromagnetic wave propagation at mobile communications frequencies," *IEEE Trans. Antennas Propag.*, vol. 49, no. 11, pp. 1590–1596, Nov. 2001.

[61] S. Shinozaki, M. Wada, A. Teranishi, H. Furukawa, and Y. Akaiwa, "Radio propagation characteristics in subway platform and tunnel in 2.5 GHz band," in *Proc. 6th IEEE Int. Symp. PIMRC*, Sep. 1995, vol. 3, pp. 1175–1179.

[62] M.-S. Choi *et al.*, "Path-loss characteristics in subway tunnels at 2.65 GHz," *Microw. Opt. Technol. Lett.*, vol. 48, no. 2, pp. 383–386, Feb. 2006. [Online]. Available: http://dx.doi.org/10.1002/mop.21357

[63] K. Guan, Z. Zhong, B. Ai, and T. Kuerner, "Propagation measurements and analysis for train stations of high-speed railway at 930 MHz," *IEEE Trans. Veh. Technol.*, vol. 63, no. 8, pp. 3499–3516, Oct. 2014.

[64] K. Guan, Z. Zhong, B. Ai, and T. Kuerner, "Empirical models for extra propagation loss of train stations on high-speed railway," *IEEE Trans. Antennas Propag.*, vol. 62, no. 3, pp. 1395–1408, Mar. 2014.

[65] K. Guan, Z. Zhong, B. Ai, and T. Kuerner, "Propagation measurements and modeling of crossing bridges on high-speed railway at 930 MHz," *IEEE Trans. Veh. Technol.*, vol. 63, no. 2, pp. 502–517, Feb. 2014.

[66] K. Guan, Z. Zhong, B. Ai, and T. Kuerner, "Propagation prediction for composite scenarios of dense semi-closed obstacles in high-speed railway," in *Proc. 31st URSI GASS*, Aug. 2014, pp. 1–4.

[67] R. He, Z. Zhong, B. Ai, and J. Ding, "Propagation measurements and analysis for high-speed railway cutting scenario," *Electron. Lett.*, vol. 47, no. 21, pp. 1167–1168, Oct. 2011.

[68] R. He, Z. Zhong, B. Ai, and J. Ding, "Measurements and analysis of short-term fading behavior for high-speed rail viaduct scenario," in *Proc. IEEE ICC*, Jun. 2012, pp. 4563–4567.

[69] L. Liu *et al.*, "Position-based modeling for wireless channel on high-speed railway under a viaduct at 2.35 GHz," *IEEE J. Sel. Areas Commun.*, vol. 30, no. 4, pp. 834–845, May 2012.

[70] Y. Zhang *et al.*, "A novel spatial autocorrelation model of shadow fading in urban macro environments," in *Proc. IEEE Global Telecommun. Conf.*, New Orleans, LO, USA, Nov. 2008, pp. 1–5.

[71] F. Luan, Y. Zhang, L. Xiao, C. Zhou, and S. Zhou, "Fading characteristics of wireless channel on high-speed railway in hilly terrain scenario," *Int. J. Antennas Propag.*, vol. 2013, 2013, Art. ID. 378 407. [Online]. Available: http://dx.doi.org/10.1155/2013/378407

[72] H. Wei, Z. Zhong, L. Xiong, B. Ai, and R. He, "Study on the shadow fading characteristic in viaduct scenario of the high-speed railway," in *Proc. 6th Int. ICST Conf. CHINACOM Netw.*, Harbin, China, Aug. 2011, pp. 1216–1220.